Preprint typeset using LaTeX style emulateapj v. 6/22/04

MID-INFRARED SPECTRA OF PAH EMISSION IN HERBIG AEBE STARS

G. C. Sloan[1], L. D. Keller[2], W. J. Forrest[3], E. Leibensperger[2], B. Sargent[3], A. Li[4], J. Najita[5], D. M. Watson[3], B. R. Brandl[6], C. H. Chen[5], J. D. Green[3], F. Markwick-Kemper[7], T. L. Herter[1], P. D'Alessio[8], P. W. Morris[9], D. J. Barry[1], P. Hall[1], P. C. Myers[10], & J. R. Houck[1]

Submitted to the Astrophysical Journal, 7 Feb. 2005; revised 6 May, 2005; accepted 23 June, 2005

ABSTRACT

We present spectra of four Herbig AeBe stars obtained with the Infrared Spectrograph (IRS)[1] on the *Spitzer Space Telescope*. All four of the sources show strong emission from polycyclic aromatic hydrocarbons (PAHs), with the 6.2 μm emission feature shifted to 6.3 μm and the strongest C−C skeletal-mode feature occuring at 7.9 μm instead of at 7.7 μm as is often seen. Remarkably, none of the four stars have silicate emission. The strength of the 7.9 μm feature varies with respect to the 11.3 μm feature among the sources, indicating that we have observed PAHs with a range of ionization fractions. The ionization fraction is higher for systems with hotter and brighter central stars. Two sources, HD 34282 and HD 169142, show emission features from aliphatic hydrocarbons at 6.85 and 7.25 μm. The spectrum of HD 141569 shows a previously undetected emission feature at 12.4 μm which may be related to the 12.7 μm PAH feature. The spectrum of HD 135344, the coolest star in our sample, shows an unusual profile in the 7–9 μm region, with the peak emission to the red of 8.0 μm and no 8.6 μm PAH feature.

Subject headings: stars: chemically peculiar — infrared: stars

1. INTRODUCTION

Herbig AeBe stars (HAeBe) are intermediate mass (2–8 $M_\odot$) analogs to the roughly solar-mass T Tauri stars (Herbig 1960; Strom et al. 1972). The number of HAeBe stars in the Galaxy depends on the selection criteria, and as a result different studies have listed as few as ∼50 (Herbig's original list included 26 stars, but see Malfait et al. 1998) or as many as several hundred (The et al. 1994). One of the more conservative definitions assigns the HAeBe name to stars of spectral type A and B (and early F) that have broadened atomic emission lines in their optical spectra (hence the "e" in "AeBe") and have infrared emission in excess of a purely photospheric spectral energy distribution. Using these criteria, Malfait et al. (1998) identified 45 HAeBe stars and published spectral energy distributions (SEDs) from UV to mm wavelengths, proposing an evolutionary scenario based on mid-infrared colors and SED structure.

Meeus et al. (2001) observed the 14 spatially unresolved sources (at all wavelengths) from the list by Malfait et al. (1998) with the Short-Wavelength Spectrometer (SWS) aboard the *Infrared Space Observatory (ISO)*. They report the detection of polycyclic aromatic hydrocarbons (PAHs) in seven of the 14 sources, proposing that the emitting PAHs are located in flared disks where the shadow of a thicker inner disk cannot attenuate the UV radiation. Acke & van den Ancker (2004) recently presented spectra from the SWS for the entire list of sources of Malfait et al. (1998), and they report the detection of PAH emission in many of them, mentioning the possibility that differences in the ionization fraction of the PAHs could help explain the structure in the 2–20 μm spectra. They also noted that emission from crystalline silicates may confuse the issue. It is also clear from the SWS spectrum of 51 Oph (HD 156843; van den Ancker et al. 2001) that emission from gas near the stars may play a significant role in shaping the mid-infrared spectra of these stars and complicating detailed studies of PAH emission in that spectral range.

Habart et al. (2004) have analyzed ground-based and ISO observations of some 30 HAeBe stars and applied a model in which the material in the disk is in vertical hydrostatic equilibrium, is heated by the central star, and contains large dust grains in thermal equilibrium with the radiation field as well as small grains and PAHs that are transiently heated. They suggest that the PAH emission is primarily from the outer disks (R∼100 AU) and that strong PAH emission is predominantly from sources that have flared disks (as earlier proposed by Meeus et al. 2001).

Li & Lunine (2003) modeled ground-based spectra of HD 141569 in the 8–13 and 17–25 μm regions using a porous, cometary-type dust model consisting of coagulated, but otherwise unaltered interstellar grains along with fully ionized PAHs. They predict the shape of the 5–25 μm spectrum, noting that there should be little emission from crystalline silicates (no more than 10% by mass fraction). Since PAHs are a significant compo-

[1] Cornell University, Astronomy Department, Ithaca, NY 14853-6801, sloan@isc.astro.cornell.edu
[2] Department of Physics, Ithaca College, Ithaca, NY 14850
[3] Department of Physics and Astronomy, University of Rochester, Rochester, NY 14627-0171
[4] Department of Physics & Astronomy, University of Missouri-Columbia, Columbia, MO 65211
[5] National Optical Astronomy Observatory, 950 North Cherry Avenue, Tucson, AZ 85719
[6] Sterrewacht Leiden, P.O. Box 9513, 2300 RA Leiden, The Netherlands
[7] Astronomy Department, University of Virginia, P. O. Box 3818, Charlottesville, VA 22903
[8] Centro de Radioastronomia y Astrofisica, UNAM, Apartado Postal 3-72 (Xangari), 58089 Morelia, Michoacan, Mexico
[9] NASA *Herschel* Science Center, IPAC/Caltech, MS 100-22, Pasadena, CA 91125
[10] Harvard-Smithsonian Center for Astrophysics, 60 Garden Street, Cambridge, MA 02138

[1]The IRS was a collaborative venture between Cornell University and Ball Aerospace Corporation funded by NASA through the Jet Propulsion Laboratory and the Ames Research Center.

nent of the interstellar medium (ISM), important to the energy balance (e.g. Allamandola et al. 1989), and are apparently necessary to accurately model the emission in HAeBe stars, it is time to closely investigate not just their presence, but the specific spectral properties of the emission features from PAHs around HAeBe stars.

High-sensitivity spectra of PAHs allowing precise band strength measurements can provide information about the structure of disks and their physical and chemical conditions. The presence or absence of PAH features may provide clues to the physical properties of the disks in HAeBe systems, such as their degree of flaring (cf. Meeus et al. 2001), and may also serve as an evolutionary clock that tracks grain processing, since there are multiple destruction paths for PAHs in disks (intense irradiation, compaction and incorporation in larger grains) but no clear formation path. The PAHs in disks around HAeBe stars most likely originate in the ISM from which the stars formed. As a significant interstellar component, PAHs may have condensed onto the ice mantles of dust grains in dense clouds that were then incorporated into protostellar nebulae. The PAHs emerge as free-flying molecules when the ice mantles of grains sublimate due to stellar irradiation or grain-grain collisions (Li & Lunine 2003). The origin of interstellar PAHs, however, is not well constrained. Suggested sources for interstellar PAHs include: (1) formation around and ejection from carbon stars (Latter 1991), (2) shattering of carbonaceous interstellar dust, or of photoprocessing of mantles on interstellar dust grains (Greenberg et al. 2000), by grain-grain collisions in interstellar shocks (Jones et al. 1996), or (3) *in-situ* formation through ion-molecule reactions (Herbst 1991). It is essential to quantify the PAH features as a diagnostic in order to distinguish between these possibilities.

We have begun a spectroscopic survey in the mid-infrared (5.2–36 μm) of 16 HAeBe stars from the sample defined by Malfait et al. (1998) using the Infrared Spectrograph (IRS; Houck et al. 2004) on the *Spitzer Space Telescope* (Werner et al. 2004). One of the goals of this study is to closely examine the PAH emission in the 5.2–14 μm spectral region. We present the first results of our study with spectra and analysis for four stars that show PAH features, no silicate features, and few other solid state features in their spectra. This has allowed a careful examination of the relative positions, strengths, and shapes of the features at 6.2, 7.7–7.9, 11.3, and 12.7 μm without concern for the effects of silicate dust grains, either amorphous or crystalline. While *ISO*/SWS and PHOT-S spectra of the four sources in our sample show PAH emission features (Meeus et al. 2001; Acke & van den Ancker 2004), the *Spitzer* IRS spectra have higher sensitivity, allowing the detailed analysis that we present here.

All four of our sources show evidence of circumstellar disks in their SEDs (Malfait et al. 1998). HD 34282 evidently has a large Keplerian disk inferred from millimeter observations (Merin et al. 2004; Pietu et al. 2003), and the disk around HD 141569 has been imaged directly in the optical and near infrared (Boccatelli et al. 2003; Mouillet et al. 2001; Weinberger et al. 1999; Augereau et al. 1999; Weinberger et al. 2005). HD 135344 has yet to be spatially resolved (Meeus et al. 2001), but Habart et al. (2005) have spatially resolved the PAH emission at 3.3 μm in HD 169142.

2. OBSERVATIONS AND ANALYSIS

The four HAeBe targets were observed with the IRS on *Spitzer* in 2004 from January to October, as described in Table 1. This paper focuses on the observations with the Short-Low module (SL), which covers the 5.2–14 μm region with a spectral resolving power of R$\sim$90. The SL slit is $3\farcs6$ (2 pixels) across and $57''$ long.

We started with the flatfielded images generated by the standard IRS data reduction pipeline (S11.0) at the Spitzer Science Center (SSC). We removed the background emission by differencing images with the source in the separate nod positions of each of the SL apertures. When extracting spectra from the images, we used an extraction window which scales with wavelength; this method is similar to that used by the SSC pipeline. We obtained a spectrophotometric calibration by using identically extracted spectra of the standard star HR 6348 (K0 III) and spectral templates of this star prepared using the methods described by Cohen et al. (2003) and modified as described by Sloan et al. (2005b). The spectra in both nods and in both SL apertures were calibrated separately and then combined into one spectrum. This method generally results in very high precision within a single spectrum, indicated by the error bars in our plots, and an absolute photometric accuracy of $\sim$10% or better.

We have modified the S11.0 version of the wavelength calibration, as described by Sloan et al. (2005a). This modification shifts the wavelength calibration in SL order 1 by 0.04 μm to the blue. We estimate that our wavelengths are accurate to better than 0.02 μm.

Figure 1 presents the spectra of our four HAeBe stars (with the spectrum of HD 135344 divided by 10 to fit on the same plot with the other three). The figure includes error bars which are generally smaller than the vertical widths of the lines used to plot the spectra. These errors are the formal uncertainty in the mean of the spectra from the two nod positions in the SL slit (half the absolute value of the difference). With the notable exception of HD 141569, which appears to have a single cool component peaking at 40 μm, the SEDs in our sample consist of a combination of a warm component peaking in the near infrared ($\sim$2 μm) and a cooler component peaking at longer wavelengths (Malfait et al. 1998). This double-peaked structure may indicate that the disks have formed significant gaps between a warm inner disk and a cool outer disk. The wavelength of the dip in intensity between the warm and cool components shifts slightly from star to star. Thus three of the spectra are flat because the wavelength region observed by SL lies more in the dip between these two components. The continuum of HD 135344 appears blue because its dip appears towards longer wavelengths than the other sources and is therefore dominated by the warm component ($T \sim 1000$ K) at the short wavelength end of our spectrum.

Figure 2 illustrates how we measure the strengths of the PAH features, using HD 141569 as an example. We have used line segments as a rough estimate of the continuum under each feature. We anchor the line segment to the spectrum on either side of each feature and integrate the residual spectrum between the two anchor points to determine the total flux in the feature (in W m^{-2}). Table 2 lists the wavelength intervals used to fit

TABLE 1
Observing information

Target	Spectral Type	$U(r)$ ($\times 10^5$)[a]	IRS Campaign	Observation Date (UT)	AOR Key
HD 34282	A0e	2.3	13	2004 Oct. 10	3577856
HD 141569	A0 Ve[b]	2.3	4	2004 Mar. 3	3560960
HD 169142	A5 Ve[b]	0.71	5	2004 Mar. 26	3587584
HD 135344	F4 Ve[b]	0.16	11	2004 Aug. 8	3580672

[a]$U(r)$ is the radiation field due to the star in units of the interstellar radiation field in the Solar neighborhood, calculated at r=100 AU.
[b]Revised spectral type from Dunkin et al. (1997).

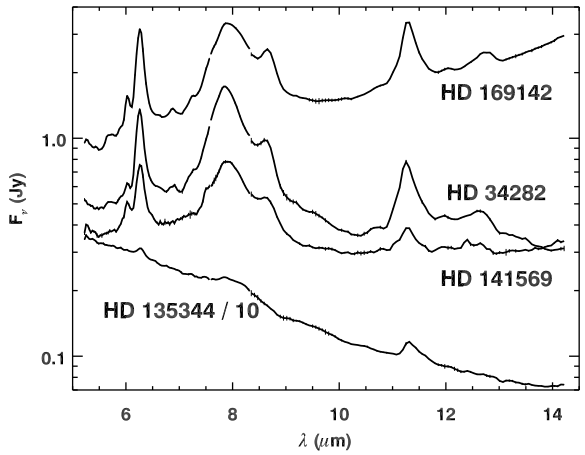

Fig. 1.— Spectra of the sample of Herbig AeBe stars showing PAH emission features and no features from silicate dust grains in their spectra. The spectrum of HD 135344 has been divided by 10. These spectra do include error bars, although they are generally smaller than the width of the lines used to plot the data.

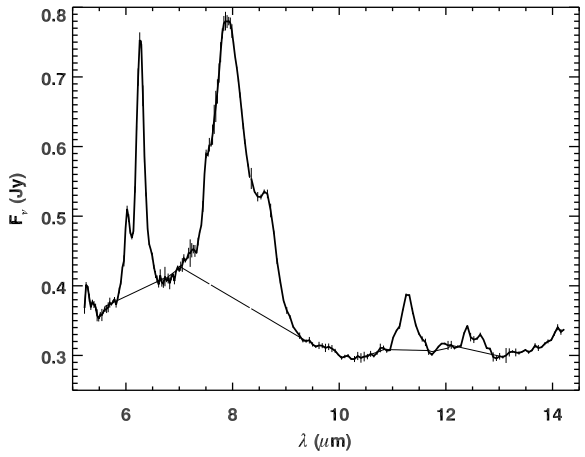

Fig. 2.— The spectrum of HD 141569 showing the linear fitting method used to measure the equivalent flux in the PAH features. Table 2 gives the wavelengths used to anchor the line segments on either side of the PAH features.

each feature. This method assumes that the PAH emission is optically thin, and it avoids dependencies on more sophisticated techniques to model the continuum. HD 135344 is the exception; before extracting the features using line segments, we first fit a polynomial estimate of the continuum to the spectrum between the features and subtract it.

TABLE 2
Fitting wavelengths

Feature (μm)	λ_{blue} (μm)	λ_{red} (μm)
6.2	5.60–5.90	6.71–6.78
7.9	6.98–7.07	9.20–9.40[a]
11.3	10.83–10.90	11.70–11.86
12.7	12.10–12.30	12.97–13.10

[a]8.85–9.05 μm for HD 135344.

We have avoided the problem of separating the PAH features from other dust features like amorphous silicate emission at 10 μm or crystalline silicate emission at 11.2 μm by choosing our sample carefully. The primary uncertainty is how much of the emission *below* the line segments belongs to the underlying PAH emission plateaux and how much belongs to the feature we are measuring. If we are truncating flux from a PAH feature, we are doing so consistently to all of the stars in the sample, and our relative measurements should remain valid.

The resulting profiles for the PAH features at 6.2, 7.7–7.9, 11.3, and 12.7 μm appear in Figures 3 and 4. Table 3 presents the total fluxes and central wavelengths for each PAH feature in each of our sources. The nominal 7.7–7.9 μm feature is shifted to 7.9 μm (or further) in our sample, so for the remainder of the paper, we will refer to this feature as the 7.9 μm feature. The reader should note that the flux labelled $F_{7.9}$ in Table 3 and plotted in following figures includes the emission of the 8.6 μm feature as well. It could be more properly described as the total PAH flux from 7 to 9 μm. We estimated the central wavelength of each feature by finding the wavelength at which half the emission lies to the blue and the red and by fitting Gaussians. The two methods produce similar results, but we adopt the Gaussian fits because they are less susceptible to noise and blended features.

Since ultraviolet and visible photons from the stellar photosphere excite the PAH emission (Li & Draine 2002), we have estimated integrated fluxes for each of our program stars, relative to the interstellar radiation field (ISRF) in the Solar neighborhood (Mathis, et al. 1983). These estimates are intended only as a guide in

TABLE 3
Feature positions and strengths

Target	6.2 μm feature λ (μm)	6.2 μm feature Flux (10^{-15} W m^{-2})	7.9 μm feature λ (μm)	7.9 μm feature Flux (10^{-15} W m^{-2})	11.3 μm feature λ (μm)	11.3 μm feature Flux (10^{-15} W m^{-2})	12.7 μm feature λ (μm)	12.7 μm feature Flux (10^{-15} W m^{-2})
HD 34282	6.26	12.63 ±0.17	7.92	47.09 ±0.58	11.27	3.11 ±0.14	12.64	0.54 ±0.06
HD 141569	6.26	6.84 ±0.15	7.98	16.65 ±0.35	11.28	0.62 ±0.10	12.52	0.18 ±0.02
HD 169142	6.26	32.71 ±0.54	8.01	88.06 ±0.93	11.30	11.86 ±0.58	12.71	1.95 ±0.17
HD 135344	6.28	3.47 ±0.51	8.02	12.49 ±1.30	11.36	1.38 ±0.21	12.75	0.18 ±0.06

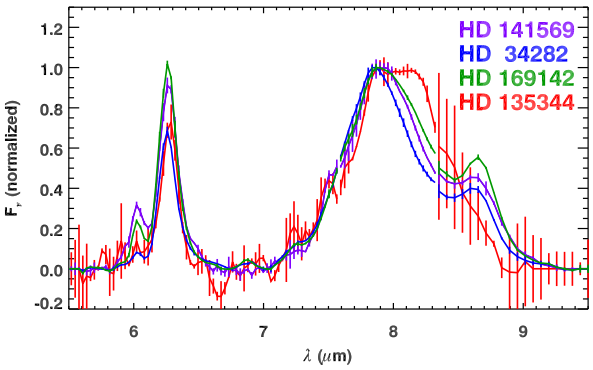

FIG. 3.— The 6.2 μm PAH emission feature and the 7–9 μm PAH emission complex (with error bars), all normalized to the peak emission in the vicinity of 8 μm. Line segments have been fit under the two emission regions and subtracted. In all four spectra, the "6.2 μm" feature has shifted to 6.3 μm, and the peak emission around 8 μm occurs at (or beyond) 7.9 μm and not 7.7 μm as often seen in other objects. The spectrum of HD 135344 shows an emission plateau from 8.0 to 8.2 μm and is missing the 8.6 μm feature.

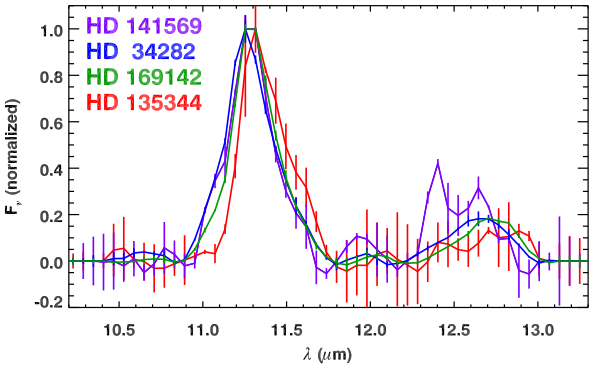

FIG. 4.— The PAH emission features at 11.3 and 12.7 μm (with error bars), after continuum subtraction. Separate line segments have been fit under the features and removed. All spectra are normalized at 11.3 μm. The most ionized spectrum, HD 141569, shows an emission feature at 12.4 μm.

our discussions of PAH excitation. Li & Lunine (2003) calculated the integrated flux (λ=0.09–1.00 μm) for HD 141569 as a function of distance, r, from the central star using spectral type B9.5 V and a Kurucz photospheric model. Table 1 presents the integrated fluxes of our stars for r=100 AU calculated relative to their value for HD 141569. Following the nomenclature of Li & Lunine (2003), $U(r) = 1$ corresponds to the ISRF in the solar neighborhood. We note that these are *not* in units of Habings or G_0, the ratio of the UV energy density to the estimate of Habing (Habing 1968), since we include the visible spectrum in addition to UV. Because the PAHs are emitting either from the surface of the disk or from the surrounding envelope, we assume no absorption between the photosphere and the PAH molecules.

3. DISCUSSION

3.1. *General spectral characteristics*

The 7.7 μm PAH feature consists of two main components, one at 7.65 μm and the other at 7.85 μm (Cohen et al. 1989; Bregman 1989; Peeters et al. 2002). The 7.65 μm feature tends to dominate the PAH spectra of reflection nebulae and H II regions where the PAHs seem to have been heavily processed. The 7.85 μm feature dominates in many planetary nebulae and objects evolving away from the asymptotic giant branch (AGB) where the PAHs seem to be relatively fresh and unprocessed. Peeters et al. (2002) studied 57 spectra of PAH sources obtained with the SWS, and they found that in spectra where the 7.85 μm component dominated, the 6.2 μm PAH feature was shifted to 6.3 μm. They used these two characteristics as the basis for what they called Class B PAH spectra.

Of the 57 spectra studied by Peeters et al. (2002), 42 belong to Class A, which shows the PAH emission features at 6.2 and 7.7 μm. Class B includes 12 spectra, and Class C, where the peak emission in the 7–9 μm range is shifted to the red of 8.0 μm, accounts for 2 sources. One source in their sample had characteristics of both Class A and B.

Figure 5 compares the spectra of HD 141569 and HD 135344 in our sample to some of the sources considered by Peeters et al. (2002). The top panel illustrates PAH spectra of Classes A, B, and C as defined by Peeters et al. (2002), using as prototypes IRAS 03260+3111 (a young stellar object in the NGC 1333 molecular cloud core), HD 44719, (the Red Rectangle), and AFGL 2688 (the Cygnus Egg), respectively. The comparison spectra were obtained from the SWS Atlas (Sloan et al. 2003). All of the IRS spectra and the SWS spectra of IRAS 03260 and HD 44179 have had the continuum removed using line segments as illustrated in Figure 2. The SWS spectra of AFGL 2688 and HD 100546 have steep red continua; to isolate the PAH spectrum we first fit a polynomial to the continuum and subtracted it.

Figure 3 and the middle panel of Figure 5 show that

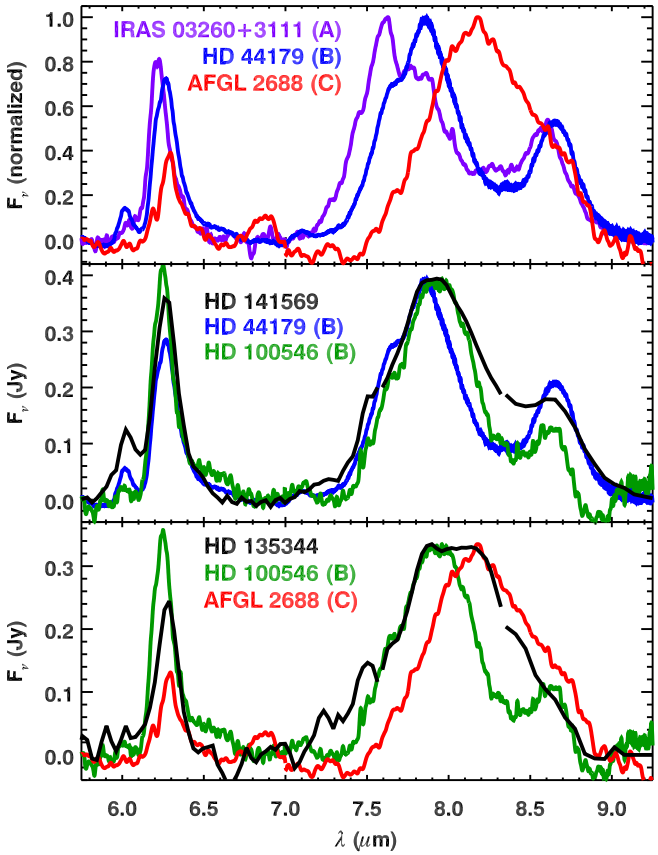

FIG. 5.— A comparison of spectra from the SWS on *ISO* with two spectra from our sample. Top: Prototypical SWS spectra of the three classes defined by Peeters et al. (2002). IRAS 03260+3111 is a young stellar object, while HD 44179 (the Red Rectangle) and AFGL 2688 (the Cygnus Egg) are post-AGB objects. Middle: HD 141569 compared to two Class B objects. HD 141569 resembles the HAeBe star more than HD 44179. Bottom: HD 135344 compared to HD 100546 and the Class C spectrum from AFGL 2688, showing that the spectrum resembles a blend between the two.

our HAeBe stars have spectral features typical of Class B, with the 6.2 μm feature shifted to at least 6.26 μm, and the peak emission in the 7.6–7.9 μm region falling near 7.9 μm. Both the 6.2 and 7.9 μm features arise from C−C stretching modes. The 8.6 μm feature, which is included in our measurements of the strength of the 7.9 μm feature, probably arises from a C−H in-plane bending mode.

The sample examined by Peeters et al. (2002) includes two isolated HAeBe stars, HD 100546 and HD 179218, both of which they included with the Class B PAH spectra. The middle panel of Figure 5 shows that in the spectrum of HD 100546, the 7.9 μm PAH feature is actually shifted to even longer wavelengths, nearly to 8.0 μm. In the other HAeBe star, this feature appears at 7.8 μm, but in all four of the IRS spectra, this feature lies closer to 8.0 μm. Thus, in five of the six isolated HAeBe stars studied here or by Peeters et al. (2002), the 7.8–7.9 μm feature indicative of Class B is shifted nearly to 8.0 μm. The HAeBe stars may represent a subgroup within Class B.

Other features visible in the spectra in Figure 1 in the 5–8 μm range require comment as well. The 5.2 μm PAH emission feature appears in three of the spectra at the short-wavelength cut-off, but it is absent in HD 34282. Two of the spectra, HD 34282 and HD 169142, show spectral structure in the vicinity of 7 μm which is due to emission features at 6.85 and 7.25 μm.

Chiar et al. (2000) made the first detection of absorption features at 6.85 and 7.25 μm, which they attributed to C−H stretching modes in aliphatic hydrocarbons such as methyl or methylene groups. This discovery was made in the SWS spectrum of Sgr A*. Bouwman et al. (2001) detected the 6.85 μm band in emission in the HAeBe star HD 163296. Spoon et al. (2004) recently reported the 6.85 and 7.25 μm bands in absorption in the spectrum of the ultraluminous infrared galaxy IRAS F00183-7111, and they showed that laboratory data of hydrogenated amorphous carbon (HACs; Furton et al. 1999) provide a good match. We note that the 3.4 μm interstellar absorption band, identified as an aliphatic C−H stretching mode (Sandford et al. 1991), can also appear in emission (Geballe & van der Ween 1990; Geballe et al. 1992). It is likely, therefore, that we have observed these aliphatic HAC features in emission in HD 34282 and HD 169142.

3.2. *HD 135344*

The spectrum of HD 135344 contains a much stronger contribution from a warm ($T \sim 1000$ K) underlying the PAHs, making the shape and position of the weaker PAH features much more susceptible to any systematic problems with the extraction and calibration of the spectrum, which explains the larger error bars in its spectrum in Figure 3. Nonetheless, some differences from the other spectra in the sample are still apparent.

In the 7–9 μm region, HD 135344 shows a plateau extending from 8.0 to 8.2 μm, most likely a blend of peaks at these two wavelengths. The 8.0 μm peak is similar to that seen in four of the other HAeBe stars, but the 8.2 μm peak more closely resembles Class C PAH spectra (Peeters et al. 2002). Both of the objects in this class, AFGL 2688 and IRAS 13416-6243, are post-AGB objects, and neither show an 8.6 μm feature. HD 135344 has more emission shortward of 8.0 μm than these two objects, but the missing 8.6 μm feature is striking.

The spectrum of HD 135344 differs from the other HAeBe stars in other ways. The 11.3 μm feature is shifted by at least 0.06 μm to the red; this is too large to arise from the random pointing errors which occasionally place a star off the central axis of the IRS slit. HD 135344 also has a relatively weak contribution 6.0 μm (compared to 6.3 μm).

Beintima et al. (1996) attributed the 6.0 μm satellite of the 6.2 μm feature to a weak C−C mode, but we note that in the objects studied by Peeters et al. (2002) the strength of the 6.0 μm feature shows no correlation with that of the 6.2 μm C−C mode. A correlation between the strength of the two bands also seems absent in our sample. Peeters et al. (2002) speculated that the 6.0 μm feature arises from C−O stretching modes in oxygenated PAH species, but these modes generally peak at somewhat shorter wavelengths (Schutte et al. 1990). The carrier of the 6.0 μm feature remains uncertain.

Oudmaijer et al. (1992) have revised the spectral classification of HD 135344 from A0 V (Houk 1982) to F4 Ve, and Dunkin et al. (1997) have confirmed this new

spectral type.[11] It is interesting that this source, which is significantly cooler than the other three sources in the sample, is the one which shows the most unusual PAH emission in the 8 μm region.

3.3. *Dependence of PAH emission on ionization fraction*

The relative strengths of PAH features can be used to identify the degree of ionization of the PAHs. They may therefore provide clues to the incident radiation field, electron densisty, and gas temperature. The most obvious difference between neutral and ionized PAHs is the relative strength of the C−C modes in the 7.7–7.9 μm region to the out-of-plane C−H bending modes at 11.3 μm and longer wavelengths (e.g. Allamandola et al. 1999). Ionized PAHs emit more strongly in the features at 6–9 μm than in the 10–13 μm region, while in neutral PAHs, the 10–13 μm region dominates. The models of Draine & Li (2001) show that the ratio $F_{7.9}/F_{11.3}$ increases with the size of the PAH molecule since larger PAHs generally have a higher C:H ratio (e.g. see Li & Draine 2001). However, a shift from neutrals to ions increases the ratio much more significantly, by a factor of ∼10.

We can thus use the ratio of the strengths of the 7.9 and 11.3 μm features as an estimate for the relative degree of ionization in each spectrum. This ratio is the most obvious difference among the spectra in our sample, varying from 7.4 in HD 169142 to 25.2 in HD 141569, making these the least and most ionized PAH spectra, respectively. The ratios for the intermediate stars are 9.1 for HD 135344 and 15.2 for HD 34282.

Recent optical spectroscopy by Dunkin et al. (1997) confirms the previous revision of the spectral classification of HD 135344, as discussed above, and also revises the classification of HD 169142 from B9 V (Houk 1982) to A5 Ve. These new classifications correlate with the observed ionization fractions as measured by the $F_{7.9}/F_{11.3}$ ratio, with the two A0 stars having the more ionized spectra, and the later-type stars having the less ionized spectra.

In HD 141569, according to detailed models (Li & Lunine 2003), the charging of PAHs is dominated by collisions with electrons and not by emitting photoelectrons. The electron recombination rate is three orders of magnitude larger than the photoelectron emission rate. For this case, then, the PAHs are negatively charged. Our analysis is not sensitive to the polarity of the charge of the PAHs, only the ionization fraction.

3.4. *The 7.9 μm feature*

There is no clear explanation for the varying strengths of the components of the 7–9 μm PAH complex among observed sources. Bregman & Temi (2005) investigate two possible causes in their study of the spatial distribution of the components in extended reflection nebulae. The peak of the complex might shift from 7.6 to 7.9 μm as the fraction of PAH cations increases or as the fraction of fresh and unprocessed PAHs increases. Our sample shows a range of ionization fractions, but in three of the four spectra, the shape of the 7–9 μm complex looks similar. The ratio of the 7.9 μm and 11.3 μm features varies by a factor of 3.7 in these three sources, and yet the relative contributions of the 7.6 and 7.9 μm components seems fixed, which would suggest that the components are not sensitive to ionization, at least over the ionization range we have examined.

The size of the PAH molecules may also influence the relative strengths of the features at 7.6 and 7.9 μm, but there is some disagreement over how the position of the strongest feature in this wavelength range will depend on PAH size. Boissel et al. (2001) suggest that very small grains produce the longer-wavelength feature, but Hudgins et al. (1999b) report that their laboratory measurements show that the 7.6 μm feature shifts to longer wavelength for *larger* PAHs. We can only say that our data are least consistent with the dependence of the 7–9 μm PAH complex on ionization fraction.

3.5. *Possible correlations with PAH size and structure*

The models of Draine & Li (2001) show a dependence of the ratio $F_{6.2}/F_{7.9}$ on the size of the PAH molecule, but it is weak, with the flux ratio doubling only when the number of C atoms has been reduced by a factor of ∼10. The top panel of Figure 6 shows that the ratio $F_{6.2}/F_{7.9}$ varies by a factor of two in our sample, but not in any systematic way with the ionization fraction as indicated by $F_{7.9}/F_{11.3}$.

To better discriminate the size of the PAH molecules, Hony et al. (2001) use the ratio $F_{12.7}/F_{11.3}$. The 11.3 μm feature arises from a C−H stretching mode when an aromatic ring contains only one H atom, such as one might find along the edge of a large PAH molecule. The 12.7 μm feature arises from the C−H trio stretching mode, i.e. from aromatic rings with three H atoms, which will be found on the corners and ends of PAH molecules. As one increases the size of a PAH molecule, the strength of the emission at 11.3 μm will increase with respect to the emission at 12.7 μm.

The bottom panel of Figure 6 shows that the strength of the 12.7 μm feature generally increases with the ionization fraction. Comparing this panel with the top panel reveals that the use of the ratios $F_{6.2}/F_{7.9}$ and $F_{12.7}/F_{11.3}$ as size indicators gives contradictory results.

The $F_{12.7}/F_{11.3}$ ratio may be influenced not just by the size of the PAHs, but by their geometry. If a compact PAH is rearranged into a structure with the same number of carbon atoms but with more uneven edges, the strength of the duo and trio modes will increase compared to the solo mode. Thus, it is possible that the the enhancement of the 12.7 μm feature could also arise from more irregularly shaped and less compact PAHs.

Measurements at the Astrochemistry Laboratory at NASA Ames Research Center have revealed no dependency of the $F_{6.2}/F_{7.9}$ ratio on the size of the PAHs (Hudgins 2004, private communication), but the Astrochemistry Laboratory has not explored a full order of magnitude in PAH size. While larger PAHs, such as those modeled by Draine & Li (2001), do show a dependence, typical PAH sizes are on the order of ∼100 carbon atoms (e.g. Li & Draine 2001), and the range in PAH sizes may

[11] Zuckerman et al. (1995) and Coulson & Walther (1995) find even later spectral types, F6 V and F8 V, respectively. Coulson & Walther (1995) point out that HD 135344 is a visual binary with the two components, SAO 206462 and 206463, separated by 20″. SAO 206463 is the brighter source and is probably the origin of the A0 V classification, but the coordinates of HD 135344 match those of the fainter SAO 206462, which is the target under consideration here.

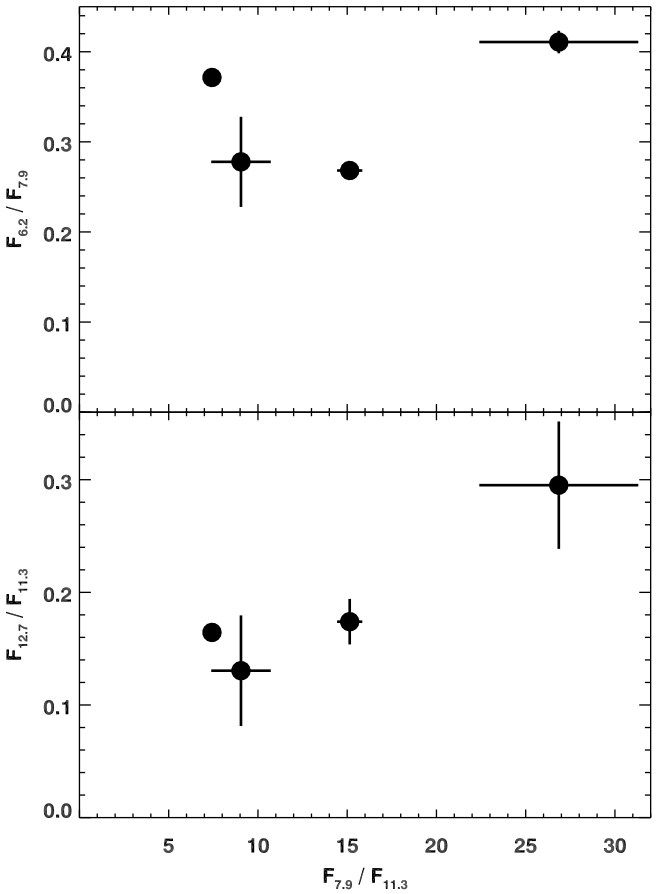

FIG. 6.— Flux ratios from the different PAH features plotted vs. the ratio of the 7.9 and 11.3 μm PAH features. The ratio $F_{7.9}/F_{11.3}$ traces the ionization fraction of the PAHs. From left to right (least to most ionized), the symbols are for HD 169142 (A5), HD 135344 (F4), HD 34282 (A0), and HD 141569 (A0). In the top panel, the relative strengths of the 6.2 and 7.9 μm features vary by a factor of $\sim$2, but they do not vary systematically with ionization fraction. The bottom panel shows that the ratio $F_{12.7}/F_{11.3}$ increases with ionization fraction, suggesting that the size of the PAHs decreases with ionization fraction.

be insufficient to dominate other causes for variation in the strength of the 6.2 and 7.9 μm bands. The relative strengths of the out-of-plane C−H bending modes, on the other hand, are much more sensitive to variations in PAH size, especially for the sizes of the molecules likely to be encountered in typical astrophysical environments.

The spectra of our HAeBe stars show other emission features in the 11–13 μm region in addition to the 11.3 and 12.7 μm features. In Figures 1 and 4, the duet out-of-plane C−H bending mode at 11.9 μm is visible in all of the spectra except HD 135344. These figures also show that what we are measuring as the 12.7 μm feature shows some structure. In the spectrum of HD 141569, the secondary emission peak at 12.4 μm actually dominates the 12.7 μm feature. The Humphreys-α line should be at 12.365 μm, but there is no corresponding Pfund-α line at 7.46 μm. The H_2 0–0 S(2) is expected at 12.28 μm, but this is too far to the blue and it is not accompanied by the 0–0 S(3) line at 9.67 μm. The most likely carrier of the 12.4 μm feature is another trio out-of-plane bending mode, as this feature can vary from 12.1 to 13.5 μm, depending on the PAH molecule (e.g. Hudgins & Allamandola 1999).

4. CONCLUSION

We have presented mid-infrared spectroscopy from *Spitzer* of four Herbig AeBe stars whose spectra show strong PAH emission but no silicate dust features. The absence of silicate emission has enabled a detailed analysis independent of specific disk models of the relative strengths and positions of PAH emission features in the 5–14 μm region.

Our sample shows spectral characteristics generally consistent with the Class B PAH emission sources identified by Peeters et al. (2002), viz. a 6.2 μm feature shifted to 6.3 μm and 7–9 μm emission dominated by the component at 7.9 μm. However, in all of our sources, the 7.9 μm feature is shifted closer to 8.0 μm, as in the spectrum of HD 100546, a HAeBe star observed by the SWS on *ISO*.

The spectra show a range in ionization fraction as revealed by the $F_{7.9}/F_{11.3}$ ratio, with HD 141569 showing the highest degree of ionization and HD 169142 the lowest. The ionization fraction is lower for later spectral classes. The strength of the 12.7 μm feature increases with respect to the 11.3 μm feature as the ionization fraction increases. The strength of the 6.2 μm feature relative to the 7.9 μm feature varies by a factor of nearly two in our sample, but in no systematic way.

The spectrum of HD 135344, the coolest star in our sample, resembles the Class C spectra discussed by Peeters et al. (2002) in some ways, with more emission to the red of 7.9 μm than in the other sources and a missing 8.6 μm feature.

Thus, our sample of PAH spectra from HAeBe stars show some characteristics which reinforce results from the literature, but also raise new questions. Why do HAeBe stars consistently produce the Class B PAH spectra seen in less than 25% of the SWS sample? What causes the shift of the 7.9 μm feature to $\sim$8.0 μm? What causes the range of 6.2 μm feature strengths compared to the 7.9 μm feature? What is the carrier of the 6.0 μm feature? Answering these questions will help us understand the nature of the HAeBe systems from which the PAH emission arises.

Quantitative measures of the size and ionization fraction of the PAHs would be valuable in determining the degree of grain processing in the disks and the fraction of short-wavelength stellar photons that reach the outer disks. With the small size of the current sample, it is not possible to determine the origin of the correlations, although we expect that the full IRS sample of HAeBe stars will bring us closer to this goal.

J. D. Bregman, D. M. Hudgins, and L. J. Allamandola provided useful comments as we prepared this manuscript. This work is based on observations made with the Spitzer Space Telescope, which is operated by the Jet Propulsion Laboratory, California Institute of Technology under NASA contract 1407. Support for this work was provided by NASA through contract number 1257184 issued by JPL/Caltech. This research has made use of the SIMBAD database operated at the Centre de Données astronomiques de Strasbourg.

REFERENCES

Acke, B. & van den Ancker, M. E. 2004, A&A, 426, 151
Allamandola, L. J., Hudgins, D. M., & Sandford, S. A. 1999, ApJ, 511, L115
Allamandola, L. J., Tielens, A. G. G. M., & Barker, J. R. 1989, ApJS, 71, 733
Augereau, J. C., Lagrange, A. M., Mouillet, & Menard, F. 1999a, A&A, 350, L51
Beintima et al. 1996, A&A, 315, L369
Boccatelli, A., Augereau, J. C., Marchis, F., & Hahn, J. 2003, ApJ, 585, 494
Boissel, P., Joblin, C., & Pernot, P., 2001, A&A, 373, L5
Bouwman, J., Meeus, G., de Koter, A., Hony, S., Dominik, C., & Waters, L. B. F. M.
Bregman, J. D. 1989, in Interstellar Dust, Proc. IAU Symp 135, ed. L. J. Allamandola & A. G. G. M. Tielens, 109
Bregman, J. D. & Temi, P. 2005, ApJ, in press
Chiar, J. E., Tielens, A. G. G. M., Whittet, D. C. B., Schutte, W. A., Boogert, A. C. A., Lutz, D., van Dishoeck, E. F., & Bernstein, M. P. 2000, ApJ, 537, 749
Cohen, M., Megeath, T. G., Hammersley, P. L., Martin-Luis, F., & Stauffer, J. 2003, AJ, 125, 2645
Cohen, M., Tielens, A. G. G. M., Bregman, J., Witteborn, F. C., Rank, D. M., Allamandola, L. J., Wooden, D., Jourdain de Muizon, M. 1989, ApJ, 341, 246
Coulson, I. M. & Walther, D. M. 1995, MNRAS, 274, 977
Draine, B. T. & Li, A. 2001, ApJ, 551, 807
Dunkin, S. K., Barlow, M. J., & Ryan, S. G. 1997, MNRAS, 286, 604
Furton, D. G., Laiho, J. W., & Witt, A. N. 1999, ApJ, 526, 752
Geballe, T. R., & van der Veen, W. E. C. J. 1990, A&A, 235, L9
Geballe, T. R., Tielens, A. G. G. M., Kwok, S., & Hrivnak, B. J. 1992, ApJ, 287, L89
Greenberg, J.M., et al. 2000, ApJ, 531, 71
Habart, E., Natta, A., & Krugel, E. 2004, A&A, 427, 179
Habart, E., Natta, A., Testi, L., Carbillet, M. 2005, A&A, in press
Habing, H. J. 1968, Bull. Astron. Inst. Netherlands, 19, 421
Herbig, G. H. 1960, ApJS, 4, 337
Herbst, E. 1991, ApJ, 366, 133
Hony, S., Van Kerckhoven, C., Peeters, E., Tielens, A. G. G. M., & Allamandola, L. J. 2001, A&A, 370, 1030
Houk, N. 1982, Michigan Catalogue of Two-Dimensional Spectral Types for the HD Stars, Vol. 3 (Ann Arbor: Univ. of Michigan)
Hudgins, D. M. & Allamandola, L. J. 1995a, J. Phys. Chem., 99, 3033
Hudgins, D. M. & Allamandola, L. J. 1995b, J. Phys. Chem., 99, 8978
Hudgins, D. M. & Allamandola, L. J. 1997, J. Phys. Chem., 101, 3472
Hudgins, D. M. & Allamandola, L. J. 1999, ApJ, 516, L41
Hudgins, D. M., Sandford, S. A., & Allamandola, L. J. 1994, J. Phys. Chem., 98, 4243
Hudgins, D. M.,& Allamandola, L. J. 1999a, ApJ, 516, L41
Hudgins, D. M.,& Allamandola, L. J. 1999a, ApJ, 513, L69
Houck, J. R., et al. 2004, ApJS, 154, 18
Jones, A. P., Tielens, A. G. G. M., & Hollenbach, D. J. 1996, ApJ, 469, 740
Latter, W. B. 1991, ApJ, 377, 187
Li, A. & Draine, B. T. 2001, ApJ, 554, 778
Li, A. & Draine, B. T. 2002, ApJ, 572, 762
Li, A. & Lunine, J. I. 2003, ApJ, 594, 987
Malfait, K., Bogaert, E, & Waelkens, C. 1998, A&A, 331, 211
Mathis, J. S., Mezger, P. G., & Panagia, N. 1983, å, 128, 212
Meeus, G., Waters, L. B. F. M., Bouwman, J., van den Ancker, M. E., Waelkens, C., & Malfait, K. 2001, A&A, 365, 476
Merin, B., et al. 2004, A&A, 419, 301
Mouillet, D., Lagrange, A. M., Augereau, J. C., & Menard, F. 2001, A&A, 372, L61
Oudmaijer, R. D., van der Veen, W. E. C. J., Waters, L. B. F. M., Trams, N. R., Waelkens, C., Engelsman, E. 1992, A&AS, 96, 625
Peeters, E., Hony, S., Van Kerckhoven, C., Tielens, A. G. G. M., Allamandola, L. J.; Hudgins, D. M., & Bauschlicher, C. W. 2002 A&A, 390, 1089
Pietu, V., Dutrey, A., & Kahane, C. 2003, A&A, 398, 565
Sandford, S. A., Allamandola, L. J., Tielens, A. G. G. M., Sellgren, K., Tapia, M., & Pendleton, Y. 1991, ApJ, 371, 607
Shu, F. H., Adams, F. C., & Lizano, S. 1987, ARA&A, 25, 23
Schutte, W. A., Tielens, A. G. G. M., Allamandola, L. J., Wooden, D. H., Cohen, M. 1990, ApJ, 360, 577
Sloan, G. C., Hayward, T. L., Allamandola, L. J., Bregman, J. D., DeVito, B., & Hudgins, D. M., 1999, ApJ, 513, L65
Sloan, G. C., Kraemer, K. E., & Price, S. D. 2003, ApJS, 147, 379
Sloan, G. C., et al. 2005, in prep.
Sloan, G. C., Spoon, H. W. W., & Bernard-Salas, J., IRS Technical Report 05002, Low-resolution wavelength calibration of the IRS (Ithaca, NY: Cornell, available at http://isc.astro.cornell.edu/tech/tr/)
Spoon, H. W. W., et al. 2004, ApJS, 154, 184
Strom, S. E, Strom, K. M., Yost, J., Carrasco, L., Grasdalen, G. 1972, ApJ, 173, 353
The, P. S., de Winter, D., & Perez, M. R. 1994, A&AS, 104, 315
van den Ancker, M. E., Meeus, G., Cami, J., Waters, L. B. F. M., & Waelkens, C., 2001, A&A, 369, L17
van den Ancker, M.E. 2000, in Disks, Planetesimals, & Planets, ASP Conf. Series 219, ed. F. Garzón, C. Eiroa, D. de Winter, & T. J. Mahoney, 242
Waters, L. B. F. M & Waelkens, C. 1998, ARA&A, 36, 233
Weinberger, A. J., et al. 1999, ApJ, 525, L53
Weinberger, A. J., et al. 2005, ApJ, submitted
Werner, M. W., et al. 2004, ApJS, 154, 1
Zuckerman, B., Forveille, T., & Kastner, J. H. 1995, Nature, 373, 494